A Study on the Performance of the Fluidic Thrust Vector Control Utilizing Supersonic Coanda Effects

MyungJun Song[1], SangHun Yoon[1], HongBeen Chang[1, 2], YongHo Cho[3], Yeol Lee[4]

1. Graduate School, Department of Aerospace & Mechanical Engineering, Korea Aerospace University
   Goyang-Si, 412-791
   Korea
   mjsong@kau.ac.kr, shyoon@kau.ac.kr
2. Agency for Defense Development
   Taejon, 305-600
   Korea
   humanchb@korea.com
3. Microfriend Inc.
   Seoul, 139-240
   Korea
   yhcho@microfriend.co.kr
4. School of Aerospace & Mechanical Engineering, Korea Aerospace University
   Goyang-Si, 412-791
   Korea
   ylee@kau.ac.kr, Corresponding author

Abstract

Co-flow fluidic thrust vector control is one of the efficient thrust-vectoring methods. The present technique controls the direction of a supersonic primary jet by utilizing coanda effects of the secondary jet exhausted at the nozzle exit. A multi-component force measurement system is developed to quantitatively evaluate the performance of the fluidic thrust control technique. Detailed calibration and data analysis have been performed to reduce measurement errors. It is found that the interaction error between load cells possibly introduced by misalignment of the test device is estimated to be less than 5%, and that the unwanted pressure errors associated with air supply tubes are negligible. Some preliminary thrust-vectoring test results and comparison with the results of flow visualization/numerical calculation are also provided. It is observed that the deflection angle the primary jet varies almost linearly with variation of the momentum ratio of the primary jet to the secondary coanda jet.

Key words: supersonic, thrust vector control, coanda effects, calibration

1. Introduction

There has been a strong demand to improve the capability of thrust vector control in supersonic rectangular nozzles in Unmanned Aerial Vehicles. A previous study showed that Fluidic Thrust Vector Control (FTVC) methods can improve the thrust capacity per engine weight by 7-12% and the operating costs by 37-53%[1], with additional advantages in nozzle cooling performances and fast response time in control[2, 3], as compared to other conventional (mechanical) control methods. Of the various FTVC methods[4-6] that have been studied to date, the method to utilize the coanda effect of the secondary flow injected at the nozzle exit becomes a

subject of interests. Some previous studies[6-8] demonstrated that the thrust vectoring technique utilizing the coanda effect works fine to deflect the primary jet's direction to some extents.

Those results, however, has been limited to control only yaw[7] in relatively low-speed subsonic regions[6]. Recent experimental[8] and numerical[9] studies also have limitations in assessing the quantitative performance-characteristics of the control technique. Therefore there is a strong need for a quantitative and accurate measurement of the performance of the co-flowing fluidic thrust vectoring control. Previous research[10-13] have shown that thrust-vectoring measurements could be substantially affected by the interaction between load cells in the test device and by the high pressure air supply lines, which requires detailed calibration and data analysis process to increase the accuracy and repeatability of the test device.

In the present work, a multi-component force measurement system using four load cells is developed to quantitatively evaluate the performance-characteristics of the thrust control technique in supersonic regime (Mach 2.0). Detailed calibration and data analysis have been performed to reduce measurement errors. An independent calibration load was used to evaluate the errors associated with to the unwanted interaction between load cells, and the additional errors caused by high-pressure air supply tubes is quantitatively evaluated for various combinations of the chamber pressures. Comparisons of the axial thrust calculated by 1-D theory with the thrust measured by the present device are also carried out to confirm the accuracy of the test device. Finally, some preliminary thrust-vectoring test results obtained by the present device are also carried out. Detailed comparisons with previous results obtained by the flow visualization and the numerical method are provided.

2. Experimental Method

2.1 Rectangular nozzle for thrust vector control

This section describes the FTVC nozzle rig developed in the present study. The schematic of the test facility layout is shown in Fig. 1. The primary and secondary high-pressure airs are supplied from an air storage tank (25atm, 3m^3). The primary chamber pressure is controlled by an electronic pressure controller (TESCOM, ER 3000SI-1), capable to maintain the constant pressure within 3% of the target values during tests.

Figure 2 shows the detailed configuration of the nozzle. The design Mach number of the two-dimensional primary nozzle flow is 2.0, and the exit Mach number of the converging secondary nozzle is 1.0. The nozzle width is 40mm, and the aspect ratio of the exit plane of the primary nozzle is 4:1. The nozzle block is designed to vary the height of the secondary nozzle (s) by movement of the flap assembly. The radius of curvature (R) of the coanda flap is also changeable to cover wide range of test cases of s/R that is possibly one of critical parameters of the present thrust-vectoring performances.

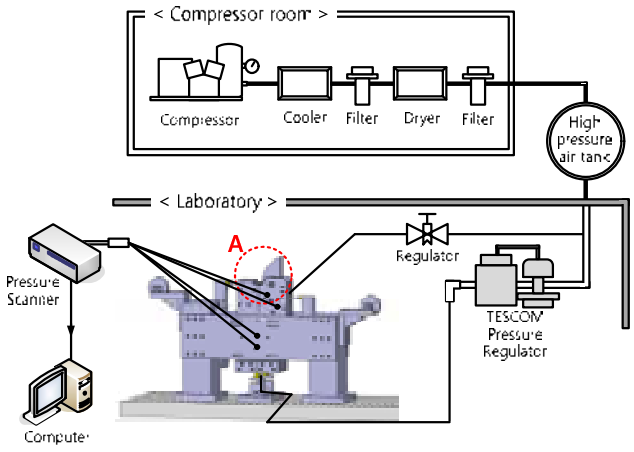

Figure 1. Layout of the present experimental set up

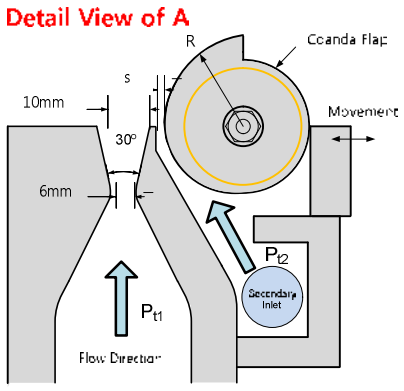

Figure 2. Schematic of the nozzle part

2.2 Design of multi-component force measurement device

The present test device is designed as vertical type that allows high accuracy measurement of normal force, and the schematic diagram of the test device is shown in Fig. 3. The test device consists of four load cells. Beam type load cell①, ②(CAS, BCA) at the side of the nozzle block measures the side force of thrust (pitch), and those are installed vertically to secure space for calibration. S type load cell③, ④(CAS, SBA) are installed at the bottom in the symmetry of the XY plane (the center plane of the primary nozzle) (see Fig. 3). Load cell③, ④ are connected in electronically parallel to be considered as one load cell. Since the interactions between the load cells due to misalignment of the device parts are main source of error in the test results[13], a right-angle ruler(RSK, squareness ±0.07mm) and laser level(±1mm/10m) are used to confirm if the test device is assembled in perfect orthogonal pattern.

Figure 4 shows the detailed configuration of thrust and force components in the FTVC assembly, where the x-axis is defined as the center line of the primary nozzle. A position of the weight attached to the side of the nozzle block is adjusted to control the center of gravity of the assembly, and thus tare load transmitted to load cell①, ② is eliminated by it. By the adjustment of the weight, the relations between thrust and component force can be simply derived as;

$$T_x = F_3 + F_4 = F_5$$
$$T_Z = F_1 - F_2 \qquad (1)$$

where F_i indicates the components of force applied to each load cell ①.

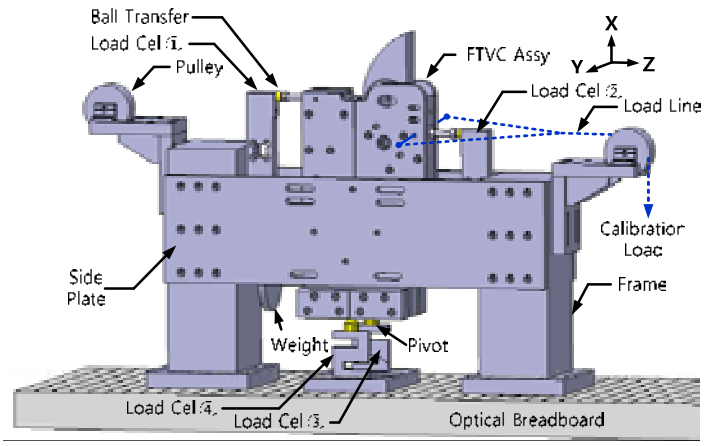

Figure 3. Layout of the force measurement device setup

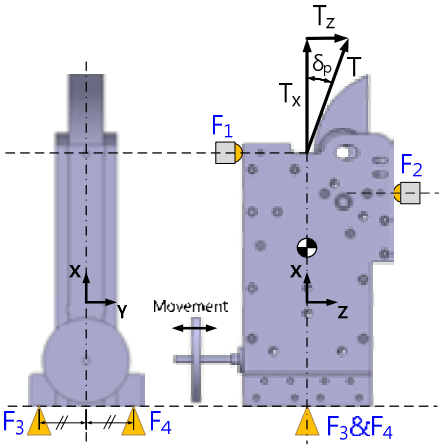

Figure 4. Configuration of thrust and force components

2.3 Data acquisition

Bridge-circuit module (NI 9237) is used to measure the signals of load cells. 10k of signal data from each load cells are acquired during 10 seconds and averaged for data analysis. The calibration weights are also weighed by a high precision electronic balance (CAS, MW-2N). Noises of the each load cell signals are also checked and it is shown that the intensity of noise-to-signal ratio is less than 1% when a load of 10kgf is applied. It is confirmed that the acquisition of each load cell signals is satisfactory and stable.

2.4 Calibration of the test device

2.4.1 Calibration of the interaction errors

Static calibrations were performed to obtain the coefficient matrix (refer the equation (2)), to account for the interaction between load cells. Independent separated calibration loads (L_1, L_2, L_5) are applied on the same axle of each load cells, as illustrated in Fig. 5. The calibration loads (L_1, L_2) are applied to calibrate load cell①, ② via an external pulley system (see Fig. 3). A physically separated calibration device is used to apply vertical calibration load (L_5) to load cell⑤.

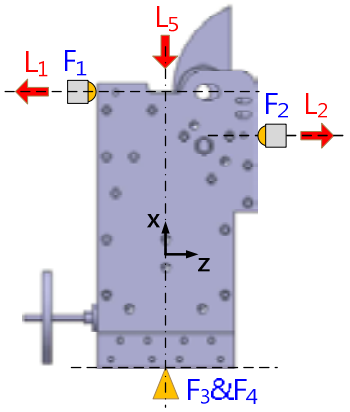

Figure 5. Schematic of the location of the calibration loads

The linear relation between the load cell signals and the actual forces is expressed as,

$$\begin{bmatrix} C_{1,1} & C_{1,2} & C_{1,5} \\ C_{2,1} & C_{2,2} & C_{2,5} \\ C_{5,1} & C_{5,2} & C_{5,5} \end{bmatrix} \begin{bmatrix} L_1 \\ L_2 \\ L_5 \end{bmatrix} = \begin{bmatrix} V_1 \\ V_2 \\ V_5 \end{bmatrix} \quad (2)$$

where matrix [C] is defined as the calibration coefficient matrix, calculated by the linear least square regression method. The subscript i in $C_{i,j}$ indicates locations of the load cell, and the subscript j indicates the locations of the calibration load. L_j is the applied calibration load and V_i is the load cell signals. Element of the calibration coefficient matrix [C] represents the weighting factor of calibration load(L_j) affecting the intensity of the load cell signal(V_i).

Evaluations of the interaction errors between load cells are performed 4 times after four re-assembles of the nozzle block. The range of calibration loads applied to each load cells has the maximum of 300N to cover the expected range of loads in actual test conditions. Four calibration data sets (Calib1~4) are obtained by getting the signals of all load cells for only one known calibration load (L_1, L_2, L_5, each) applied independently.

In the present study, the error of element of component force is defined as,

$$Error_{i,p} = \frac{L_{i,p} - L^*_{i,p}}{L_{i,p}} \times 100\% \quad (3)$$

where $L_{i,p}$ is the applied calibration load and $L_{i,p}^*$ is the calculated force using the load cell signal. The subscript i here indicates the location of the calibration load. The maximum errors of each component force(F_i) assessed by the equation (3) are shown in Table 1. It is shown that error of the load cell⑤ is less than approximately 0.3% for all conditions, proving that the accuracy of load cell⑤ is exceedingly good. The maximum error of the load cell①, ②, that is most critical in measurement of the pitch, is approximately 5% against the calibration load of 10N, showing that the good accuracy of the present test device for most loading conditions. Standard deviations and the repeatability of each elements of the coefficient matrix are also proved as small as less than 1%. For all calibration loading conditions, the interaction coefficients (off-diagonal term of the matrix [C]) were less than 1% of the direct coefficients (diagonal term of the matrix [C]). From the present detailed error analysis, it is conclude that the test device developed in the study is far better in measurement accuracy as compared to the test device presented in the previous research[12].

Table 1. Maximum error of the calibration loads

$Error_{max}$	F1	F2	F5
Calib 1	1.2%	5.3%	0.3%
Calib 2	0.9%	1.2%	0.3%
Calib 3	3.3%	2.1%	0.1%
Calib 4	1.9%	1.5%	0.1%

2.4.2 Calibration of errors of pressure loads

High-pressure air supply tubes are pressurized during the performance tests, and the unwanted forces transmitted to load cells can introduce substantial errors. In the present study, flexible tubes are used to minimize those pressure loads and the axis of the supply line is anchored to remain in right-angle to the direction of thrust[13]. The pressure load is also simulated by blocking air flow in the stagnation chamber as shown in Fig. 6. A spreader installed to stabilize the primary flow is replaced as a blocking plate as shown in Fig. 6-(a), and the secondary flow is blocked by a long cap, as illustrated in Fig. 6-(b).

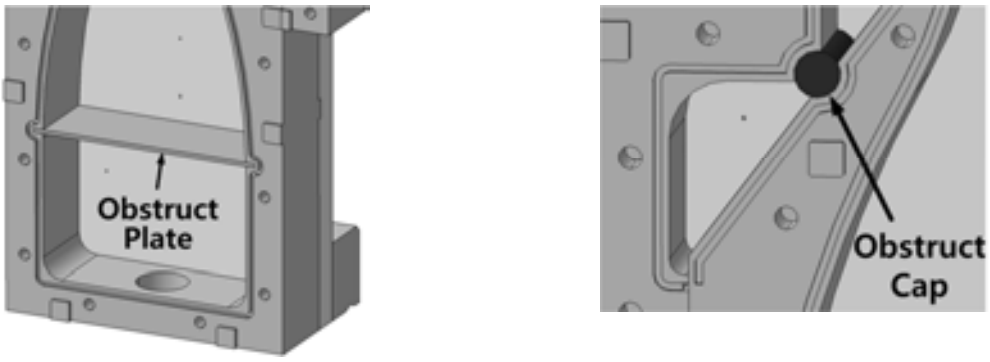

(a) blocking the primary flow **(b) blocking the secondary flow**

Figure 6. The method to block the primary/secondary flows

The range of applied pressures with the blocking plate installed covers up to 780kPa for the primary nozzle (about 780kPa) and up to 400kPa for the secondary nozzle. Each chamber is independently pressurized for various pressure conditions, and the measured component forces for each pressure loads are shown in Table 2. In the table, it is obvious that the component forces measured by the load cells are less than 1N, which is almost negligible. Since two chambers are pressurized at the same time in actual tests, the load cell signals are also observed for the cases that two chambers are all pressurized simultaneously in various pressure combinations. Similar results are observed such that the component forces measured by the load cells are less than 1N. Finally, it is proved that the magnitude of the error associated with the supplied air tubes is negligible, considering the range of expected axial/side thrusts in actual tests.

Table 2. Results of measured pressure loads introduced by air supply tubes

Primary nozzle blocked				Secondary nozzle blocked			
Pressure (kPa)	Load (N)			Pressure (kPa)	Load (N)		
P_{t1}	F1	F2	F5	P_{t2}	F1	F2	F5
400	-0.12	0.04	0.43	200	-0.08	0.05	0.17
600	0.35	0.04	0.58	300	-0.17	0.05	0.08
700	0.47	0.05	0.71	400	0.14	0.05	0.00
800	0.48	0.04	0.89				

3. Results and Discussion

3.1 Flow visualizations and numerical results

In Fig. 7 the results from flow visualization (shadowgraph) shows the characteristics of the supersonic primary jet associated with coanda effects of the secondary jet exhausted at the nozzle exit. The deflection angle (δ_p) measured by the present test device is also depicted in the figure. Figure 7 suggests that flow visualization results are qualitatively good to observe the deflection angle of the primary jet. It is also noticed that the deflection angle of the primary jet is influenced by s/R, however, further detailed study is required to evaluate the effects of the slot height of the secondary jet (s) and the radius of curvature of the coanda flap (R) independently.

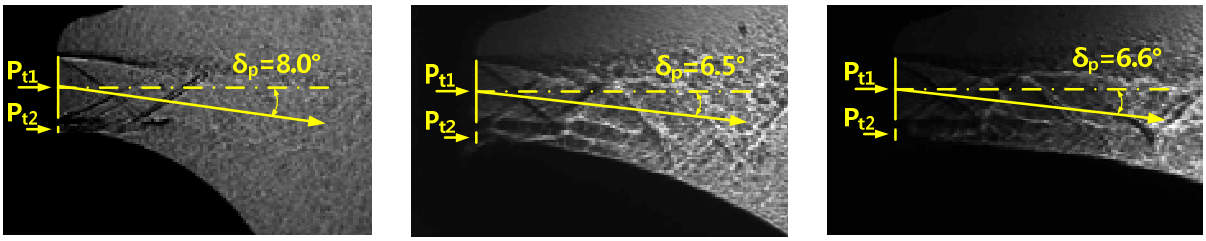

(a) s/R=0.025 (s=1mm, R=40mm) **(b) s/R=0.02 (s=2mm, R=100mm)** **(c) s/R=0.01 (s=2mm, R=200mm)**

Figure 7. Flow visualization of supersonic coanda flows (shadowgraph, P_{t1}=500kPa, P_{t2}=300kPa)

Flow visualization and numerical results are also compared as shown in Fig. 8. The present numerical results showing the variation of density gradients in the flow fields reveals a good agreement with the flow visualization results.

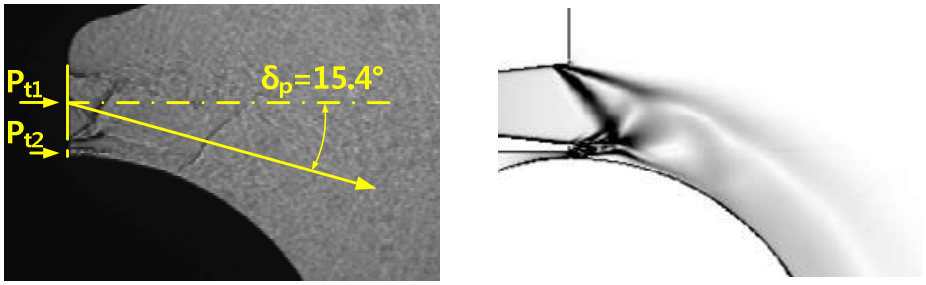

(a) P_{t1}=300kPa, P_{t2}=200kPa

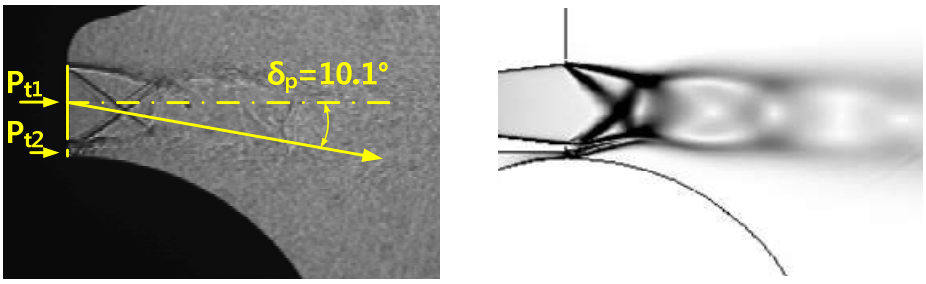

(b) P_{t1}=400kPa, P_{t2}=200kPa

Figure 8. Thrust vectoring angles of FTVC nozzle(s/R=0.025)

3.2 Comparison with the 1-D theoretical thrust

The accuracy of the present test device is validated again by comparing the measured thrust of the primary nozzle with the calculated thrust using 1-D theory of the compressible flows. In the process, the nozzle divergence coefficient[14] is introduced to account for the effects of divergence of the nozzle. Comparison of the un-vectored (axial) thrust measured in over-expanded conditions with 1-D theoretical is shown in Table 3. In the tale, it is confirmed that the measured values agrees well within 5% with calculated theoretical values, demonstrating the present test device has good measurement accuracy.

Table 3. Comparison of the measured and the theoretical thrusts

Primary chamber pressure (kPa)	Load (N)		Error (%)
	1-D calculation	Present measured (F5)	
296	58.12	61.032	5.010896926
383	86.97	87.023	0.066265971
		87.564	0.688363955
		87.274	0.354038557
		88.750	2.052123788
497	124.76	126.709	1.558579023
		125.615	0.682492808
		124.427	-0.270267003
591	155.93	155.528	-0.260286729

3.3 Deflection angles for various momentum ratios

Thrust vectoring angles of the primary jet are presented in Fig. 9 for various momentum ratios of the primary to the secondary coanda jet. Here the momentum ratio is defined as,

$$\text{Momentum Ratio} \equiv \frac{\dot{m}V_{e2}}{\dot{m}V_{e1}} = \frac{\gamma P_{0,2} A_{e,2}\left(1+\frac{\gamma-1}{2}\right)^{\frac{\gamma}{1-\gamma}}}{\gamma P_{0,1} A_{e,1} M_e^2\left(1+\frac{\gamma-1}{2}M_e^2\right)^{\frac{\gamma}{1-\gamma}}} \quad (4)$$

where γ is the specific heat ratio of air, M_e is the Mach number of primary flow at the exit plane(M_e=2.0 in the present study), and $A_{e,1}$, $A_{e,2}$ are the exit area of the primary nozzle and the secondary nozzle, respectively. In Fig. 9 it is shown that the thrust angle increases almost linearly as the momentum ratio increases for s/R=0.025 flap (see Fig. 9-(a)). Similar tests for different value of s/R=0.02 also shows the linear relation, as shown in Fig. 9-(b). For the same momentum ratio, the lower secondary pressures result in larger deflection angles, and thus it is presumed that the coanda effect in under-expanded secondary jet is not that strong.

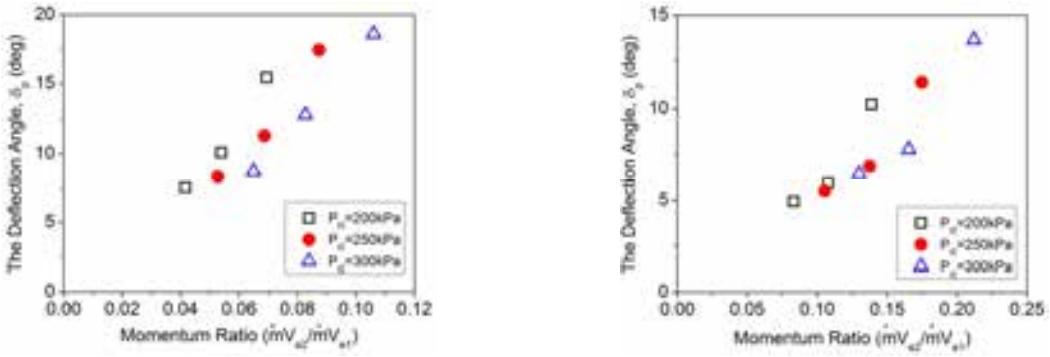

(a) s/R=0.025 (s=1mm, R=40mm) **(b) s/R=0.02 (s=2mm, R=100mm)**

Figure 9. Thrust vectoring angles of FTVC nozzle

Detailed performances of the coanda nozzle are observed for various pressures and combinations of the secondary nozzle height (s) and the radius of curvature of coanda flap (R), and its results are summarized in Fig. 10. In the figure, it is observed that the deflection angle is decreased as the pressure ratio (P_{t2}/P_{t1}) increases and that the deflection angle for the maximum value of s/R (=0.025) is relatively larger as compared to the other cases. However, any specific consistent pattern in the variation of the deflection angle with s/R is not found.

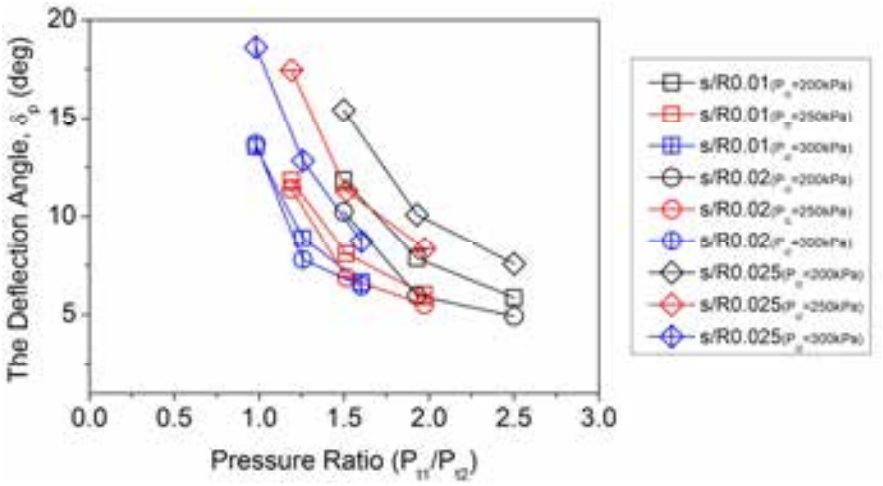

Figure 10. Thrust vectoring angles for various pressure ratios

It is obvious that the ratio of s/R is one of the influencing parameters in the performance of the coanda nozzle, but it is presumed that s/R is not only one sufficient parameter to reflect the performance of the fluidic thrust vector control. Even the decrease of s/R qualitatively weakens the performance of the primary jet's deflection, further detailed study is required to evaluate the effects of the slot height of the secondary jet and the radius of curvature of the coanda flap independently.

4. Conclusions

A multi component force test device is developed to measure the accurate and quantitative performance of the supersonic coanda nozzle. Detailed calibration and data analysis regarding the measurement accuracy of the test device reveals that the maximum measurement error of the device is less than about 5%, which shows the good accuracy and precision of the present measurement system. Unwanted pressure loads from pressurized air tubes are found to be less than 1N and thus the error associated with the air supply tubes are negligible. It is also noticed that the measured thrust values are close to the theoretical values within 5%.

Flow visualizations and numerical calculations are also carried out, and those results are compared to preliminary thrust-vectoring test results. It is shown that the flow visualization results are qualitatively good to observe the deflection angle of the primary jet, and that the results from numerical calculations are in fairly good consistency with the estimation by flow visualization.

Preliminary thrust-vectoring tests show that the variation of deflection angles of the primary jet increases almost linearly as the momentum ratio increases. It is also noticed that the decrease of s/R weakens the performance of the primary jet's deflection; however, further detailed study is required to evaluate the effects of the slot height of the secondary jet and the radius of curvature of the coanda flap independently.

Acknowledgments

This research was supported by Basic Science Research Program through the National Research Foundation of Korea (NRF) funded by the Ministry of Education, Science and Technology (2012R1A1A2006348).

References

[1] K. A. Deere: Summary of Fluidic Thrust Vectoring Research Conducted at NASA Langley Research Center. AIAA 2003-3800, 2003.

[2] C. Chiarelli, R. K. Johnsen, C. F. Shieh, D. J. Wing: Fluidic Scale Model Multi-plane Thrust Vector Control Test Results. AIAA 93-2433, 1993

[3] I. E. Diaz-Guardamino: Combining Suction Control and Transverse Jets for Fluidic Thrust Vector Control. *ProQuest*, 2008.

[4] D. J. Wing: Static Investigation of Two Fluidic Thrust-Vectoring Concepts on a Two-Dimensional Convergent Divergent Nozzle. *NASA Technical Memorandum 4574*, 1994.

[5] J. D. Flamm: Experimental Study of a Nozzle Using Fluidic Counterflow for Thrust Vectoring. AIAA 98-3255, 1998.

[6] M. S. Mason, W. J. Crowther: Fluidic Thrust Vectoring for Low Observable Air Vehicle. AIAA 2004-2210, 2004.

[7] F. Saghafi, A. Banazadeh: Coflow Fluidic Thrust Vectoring Requirements for Longitudinal and Lateral Trim Purpose. AIAA 2006-4980, 2006.

[8] S. H. Yoon, D. H. Jun, J. Y. Heo, H. G. Sung, Y. Lee: Experimental Study of Thrust Vectoring of Supersonic Jet Using Co-flowing Coanda Effects, *Journal of The Korean Society Aeronautical and Space Sciences*, Vol. 40, 2012 (to be published).

[9] S. H. Yoon, D. H. Jun, M.J. Song, Y. H. Cho, Y. Lee: Numerical Investigations on the Performance-Improvement of Fluidic Thrust Vector Controls, Proceeding of the KSME 2011 Spring Annual Meeting, 2011.

[10] A. J. Neely, F. N. Gesto, J. Young: Performance Studies of Shock Vector Control Fluidic Thrust Vectoring. AIAA 2007-5086, 2007.

[11] K. J. Lee, I. S. Park, Y. K. Choi: Design Method of the High Accuracy Thrust Stand. *Journal of the Korean Society of Propulsion Engineers*, Vol. 10, No. 1, pp.9~17, 2006.

[12] M. A. Ramaswamy, F. S. Alvi, A. Krothapalli: Special 6-Component Jet Rig Balance for Studying New Thrust Vectoring Concetps. Record International Congress on Instrumentation in Aerospace Simulation Facilities, pp.202~213, 1997.

[13] R. B. Runyan, J. P. Rynd, Jr., J. F. Seely: Thrust Stand Design. AIAA 92-3946, 1992.

[14] J. J. Berton: Divergence Thrust Loss Calculations for Convergent-Divergent Nozzles: Extensions to the Classical Case. *NASA Technical Memorandum 105176*, 1991.

[15] J. D. Flamm, K. A. Deere, M. L. Mason, B. L. Berrier, S. K. Johnson: Design Enhancements of the Two-Dimensional, Dual Throat Fluidic Thrust Vectoring Nozzle Concept. AIAA 2006-3701, 2006.